Short Communication

Effect of Carbon Nanotubes on the Electrochemical Performance of LiFePO₄ Particles in Lithium Ion Batteries

Wangjun Feng[1,2,] ,Yue Cao[2], Xing Zhao[2],Juntao Gang[2],Wenxiao Su[2]*

[1] State Key Laboratory of Advanced Processing and Recycling Nonferrous Metals, Lanzhou University of Technology, Lanzhou 730050, China;
[2] School of Science, Lanzhou University of Technology, Lanzhou 730050, China)
[*]E-mail: wjfeng@lut.cn

The pure LiFePO₄ (LFP) materials were successfully obtained via an effective and controllable hydrothermal method with the assistance of ethylene glycol (EG).Then, the LFP/carbon nanotubes (CNTs) composite was synthesized in the process of final heat treatment. X-ray diffraction (XRD) and transmission electron microscopy (TEM) were used to research the composition, morphology and structure of LFP/CNTs composite. Electrochemical performance tests demonstrated that the 4wt% carbon nanotubes composite exhibited the best discharge specific capacity. The special capacity was 154.6mAh/g at 0.1C, and it had any damping after 5 cycles. The particle size of initial LFP prepared by hydrothermal method with the assistance of EG is shorter than others. The LFP/CNTs composite formed a three-dimensional network structure that enhanced the electrochemical performance.

1. INTRODUCTION

In recently years, lithium ion battery has widely used as alternative energy sources for mobile electronic devices, electrical vehicles (EVs) and hybrid electrical vehicles (HEVs) [1,2] because of its advantages, such as light quality, high energy density, excellent cycle performance, etc [3]. Among numerous lithium ion battery cathode materials, the olivine LFP has a rapid development and become a hot research since the first report from Padhi in 1997 [4]. Comparing with other lithium ion battery cathode materials, the olivine LFP seems to be one of the most promising materials because of its low cost without noble element, flat voltage profile (3.4V), long cycle stability, relatively large theoretical specific capacity (170mAh/g), especially a superior safety performance [5–9]. However, the intrinsic

low Li^+ transport velocity and poor electronic conductivity limit the commercial use of LFP for EVs and HEVs.

The olivine-type structure of LFP consists of a hexagonal closed-packing of oxygen atoms with Li^+ and Fe^{2+} located in half of the octahedral sites and P^{5+} in 1/8 of the tetrahedral sites [10]. This structure may be described as chains of edgesharing FeO_6 octahedra that are cross-linked by the PO_4 groups forming a three dimensional network. According to the arrangement of lithium ion which tunnels along the [010] direction that demonstrate that the transport is good to improve the high rate performance of LFP [11–13]. Currently, the poor electronic conductivity limit the commercial use of LFP, therefore, the urgent task is to improve its electronic conductivity. In order to improve the electrochemical performance, extensive efforts have been made to overcome this problem, including carbon coating, reduction of particle size to nano-scale and cations doping. The LFP/CNTs composite was synthesized in the process of final heat treatment that added different percentages of CNTs [14,15].

Cations doping is a common way to improve the material conductivity, but the doping of LFP has been a hot debate. Therefore, surface coating becomes an effective method to improve the electronic conductivity, especially the carbon coating which improves the low electronic conductivity of LFP, and promotes the industrialized application [16–19]. Zhou [20] successfully prepared crystalline LFP nanoplates with 5wt% multi-walled CNTs by a facile low temperature polyol process. Guan Wu [21] used CNTs as the conducting additive in LFP and $LiCoO_2$ electrodes. The reversible discharge capacity of LFP/CNTs composite cathode was 155mAh/g at 0.1C. Tan [22] had made LFP microspheres that embedded homogeneously with three-dimensional CNTs conductive via an effective and controllable hydrothermal method using the assistance of polyethylene glycol. The test found that initial discharge capacities of the composites was about 150mAh/g at 0.1C. The LFP@CNT core-shell nanowires prepared by Wang [23] that exhibited a high capacity of 132.8mAh/g at a rate of 0.2C. In order to achieve an excellent electrochemical performance, the active material must have a nano particle size with a uniform size distribution and high crystallinity as well as high purity, short diffusion paths for ionic transport and electronic conduction.

Herein, we present the construction of 3D LFP/CNTs cathode materials, which CNTs networks coat and connect the LFP nano-particles, by the hydrothermal method with the assistance EG. The use of EG can limit the growth of LFP particles and help to generate homogeneous structure. What is more, the 3D network structure can provide abundant nano-transport pathways and reduce diffusion distance of electronic and Li^+ [24].

2. EXPERIMENTAL

2.1. Material preparation

The original materials employed in this study were $LiOH·H_2O$ (AR, Tianjin Baishi Chemical Co. ltd, TBCCI), $FeSO_4·7H_2O$ (AR, Shanghai Chemical Reagent Company, SCRC), $C_6H_8O_6$ (AR, SCRC), H_3PO_4 (AR, TBCCI), Ethylene glycol (AR, SCRC) and CTNs (Beijing Cnano Technology

Limited). Firstly, the raw materials were prepared that the stoichiometric of $LiOH \cdot H_2O$, $FeSO_4 \cdot 7H_2O$ and H_3PO_4 were 3:1:1 in mole, then, $FeSO_4 \cdot 7H_2O$ and $C_6H_8O_6$ were orderly dissolved in ethylene glycol to form a homogeneous solution under vigorous stirring, meanwhile $LiOH \cdot H_2O$ was also dissolved in ethylene glycol to form a homogeneous solution under the same condition. After 30 minutes, the solution of $LiOH \cdot H_2O$ was added slowly into $FeSO_4 \cdot 7H_2O$ suspension under vigorous stirring, then, the H_3PO_4 were dropped into it. The mixture was stirred 30 minutes, and subsequently the mixture was transferred into a 100ml Teflon-lined stainless steel autoclave and heated at 200℃ for 6h. After cooling to room temperature, the precipitates were collected by centrifugation and washed several times with distilled water and ethanol, followed by drying at 80℃ for 24h. The raw LFP was obtained by annealing at 600℃ for 10h in a nitrogen atmosphere with a heating rate of 5℃/min.

LFP/CNTs composite was synthesized in the process of annealing. The preceding LFP mixed with different percent CNTs (respectively, 1wt%, 4wt%, 7wt%, 10wt%). Subsequently, the LFP/CNTs was synthesized by annealing at 600℃ for 5h in a nitrogen atmosphere with a heating rate of 5℃/min.

2.2. Characterization

The crystal phase of all the samples were characterized by powder X-ray diffraction (XRD) using Bruker D8 Advance diffractometer with Cu Kαradiation from 10º to 80º. Transmission electron microscopy (TEM) image was obtained with a JEM -2100Fsystem operated at 200 kV.

2.3. Electrochemical analysis

Electrochemical performances of the LFP/CNTs composites were evaluated using CR2025 coin-type cell with lithium metal as the counter electrode. To prepare working electrode, the mixture of the active material, acetylene black and Polyvinylidene Fluoride (PVDF) with a weight ratio of 80:10:10 were added in N-methylpyrrolidone (NMP) solvent to form homogeneous slurry. The obtained slurry was coated on an aluminum foil, dried 10h in a vacuum oven at 120°C. The cells were assembled in a glove box filled with high-purity argon. The Land CT2001A battery test system (Wuhan, China) was used for the charge-discharge tests between 2.4 V and 4.3 V at room temperature.

3. RESULTS AND DISCUSSION

3.1. Crystalline structure analysis

The XRD patterns of all the as-prepared composites as well as pure LFP and CNTs are shown in Fig.1. It can be seen that the diffraction peaks of all the samples can be majorly assigned to pure LFP structure (JCPDS NO.40-1499).The peaks of LFP/CNTs composite indicate that the phases formed in the products are of good crystallinity. No characteristic peaks from CNTs or carbon are observed, most probably due to the low content of CNTs or carbon, which show that the additions have no obvious impact on the structure of LFP.
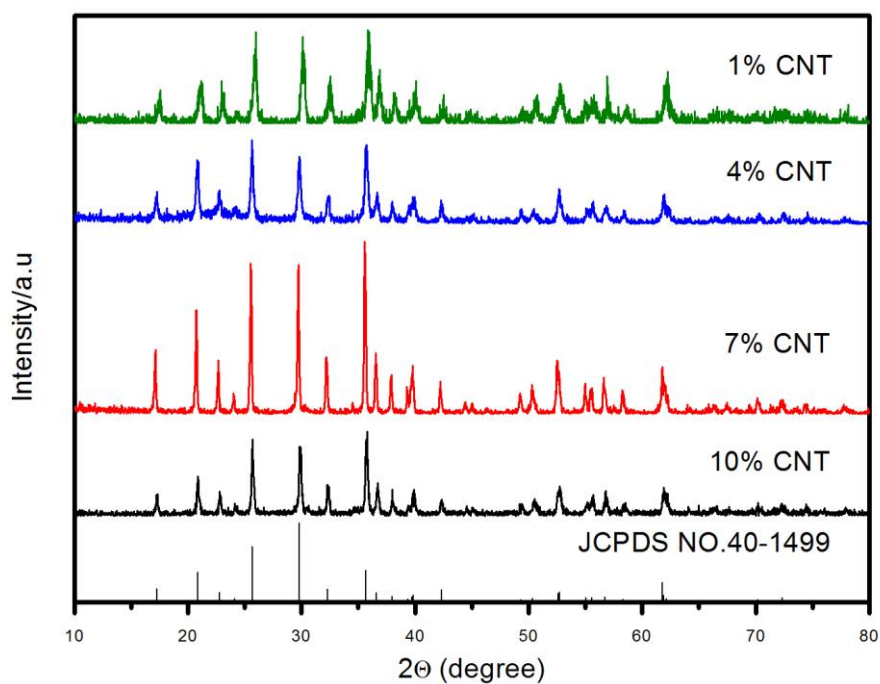
Figure 1. XRD patterns of various LFP at different contents of CNTs: (a) 1wt%, (b) 4wt%, (c) 7wt%, (d) 10wt%
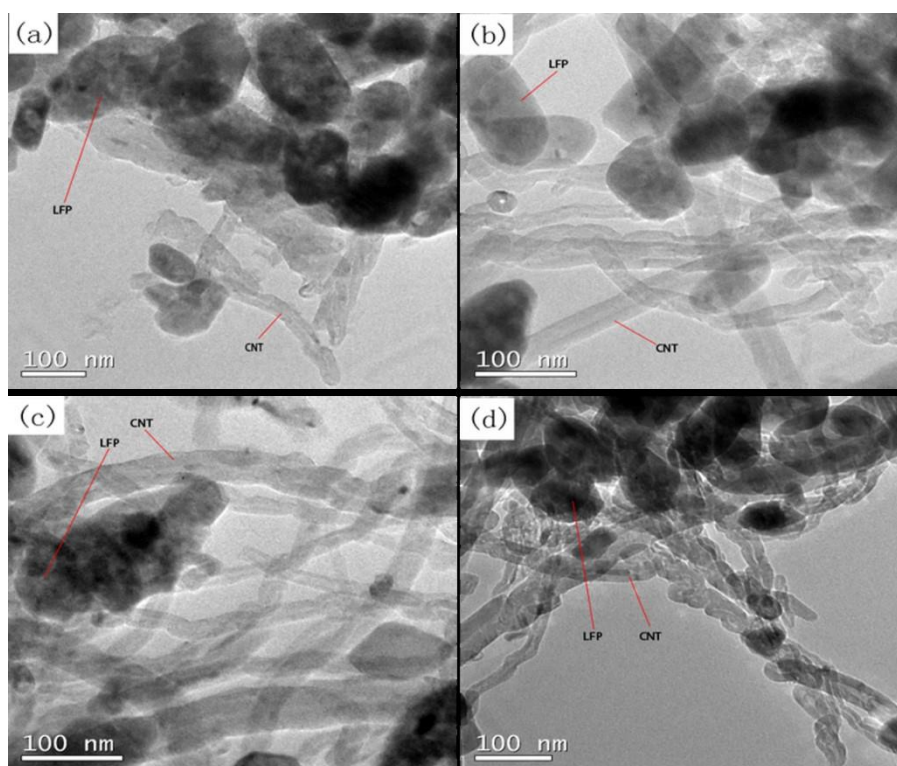
3.2 Morphological observation

Figure 2. TEM images of various LFP/CNTs: (a) 1wt%, (b) 4wt%, (c) 7wt%, (d) 10wt%

Fig.2. displays the transmission electron microscopy (TEM) images of LFP/CNTs. According to the TEM images (Fig.2.), many LFP grains are aggregated about 50-100nm in diameter. The CNTs about 20-30nm in diameter are uniformly distributed around the LFP powers that form a 3D network structure[25]. It can be seen from Fig.2 (a) (1wt%, LFP/CNTs) that the addition of CNTs are less, therefore it is difficult to find obvious 3D network structure. Obviously, the moderate 3D network structure of CNTs can be detected in Fig.2 (b) (4wt%, LFP/CNTs), which intimate contact with LFP and provide an effectively channel for Li$^+$ [26]. When the CNTs content is 7wt% in Fig.2 (c), it forms a tight and overlapping network. In Fig.2 (d) (10wt%, LFP/CNTs), an unsystematic and overlapping network is formed that caused by the excess percent contents of CNTs.
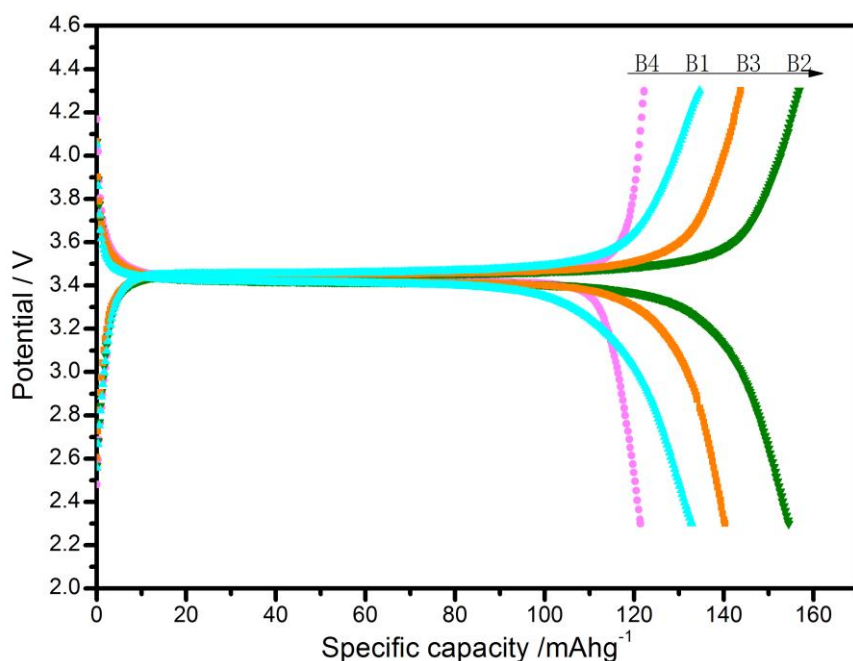
3.3 Electrochemical performances

Figure 3. The charge-discharge curve of various LFP/CNTs at 0.1C rate: 1wt%, 4wt%, 7wt%, 10wt%

The charge-discharge analysis of LFP/CNTs at 0.1C rate has been performed under the room temperature that is shown in Fig.3. All the samples are marked as B1, B2, B3 and B4 (respectively, 1wt%, 4wt%, 7wt% and 10wt%). The discharge capacity of B is observed as 154.6mAh/g, which exhibit the highest initial discharge capacity, the capacity retention is 90.9%. The sample is better than mesoporous LFP microspheres embedded homogeneously with 3D CNTs conductive networks, which the initial discharge capacity is 150mAh/g [22]. However, the discharge capacity of B4 is only 122.6mAh/g that is the lowest in all samples. The reason is that the excess CNTs are used in active

materials so that the current density is very large that reduced the discharge capacity in the process of charging and discharging[23].
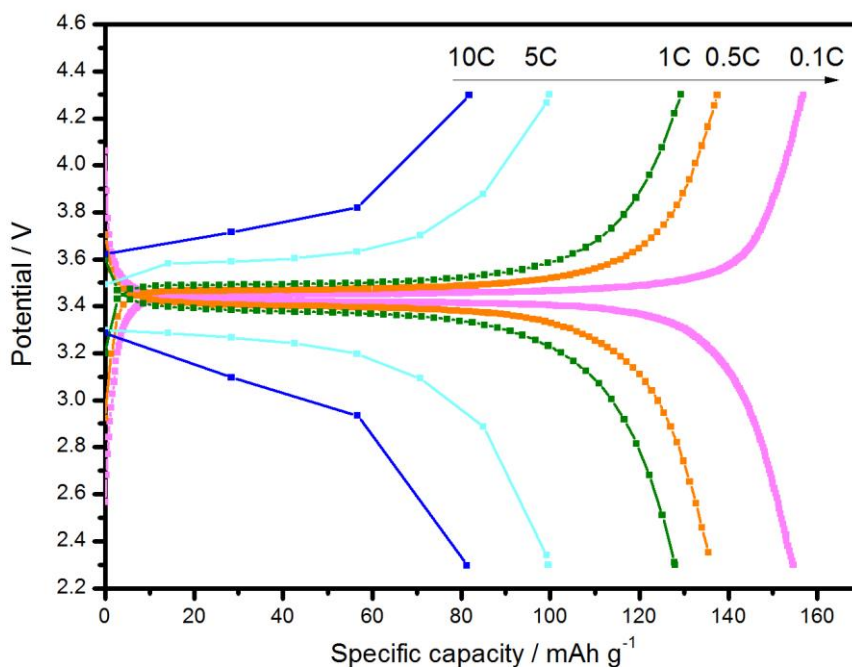
Figure 4. The charge-discharge curve of 4wt% CNTs at different rates: 0.1C, 0.5C, 1C, 5C, 10C
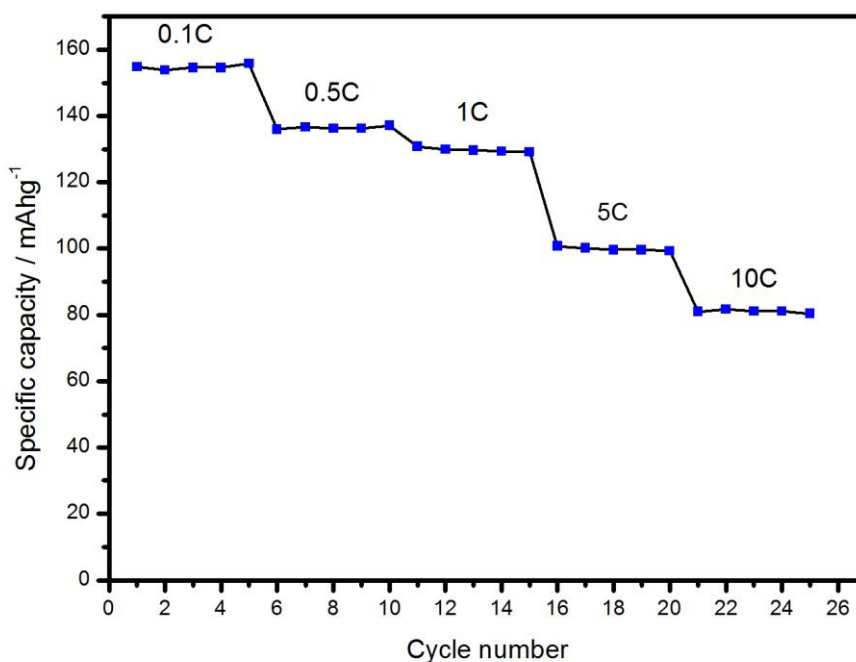
Figure 5. The cycling performances of 4wt% CNTs at different rates: 0.1C, 0.5C, 1C, 5C, 10C

The sample which the amount of CNTs is 4wt% is detected the charge-discharge capacity at 0.1C, 0.5C, 1C, 5C and 10C that shown in Fig.4. The discharge capacities of the sample are

154.6mAh/g, 135.5mAh/g, 128mAh/g, 99.6mAh/g and 81.2mAh/g at 0.1C, 0.5C, 1C, 5C and 10C, respectively. According to the curve, the material charge-discharge specific capacity gradually reduced with the increase of charge-discharge rate. The reason is that the corresponding current density and the polarization are increasing that make the discharge specific capacity continually reduce, which caused by the increase of charge-discharge rate[27,28]. The discharge capacity of the battery is lowest that almost has any discharge platform, it may be the battery depart from the thermodynamic equilibrium.

The cycling and rate performance of the sample (4wt% CNTs) are also investigated at different rates in Fig.5.The material charge-discharge specific capacity has any remarkable changes after 5 cycles at different rates, because the particle size of LFP is short and the 3D network structure improve the conductivity performance of the battery [16].
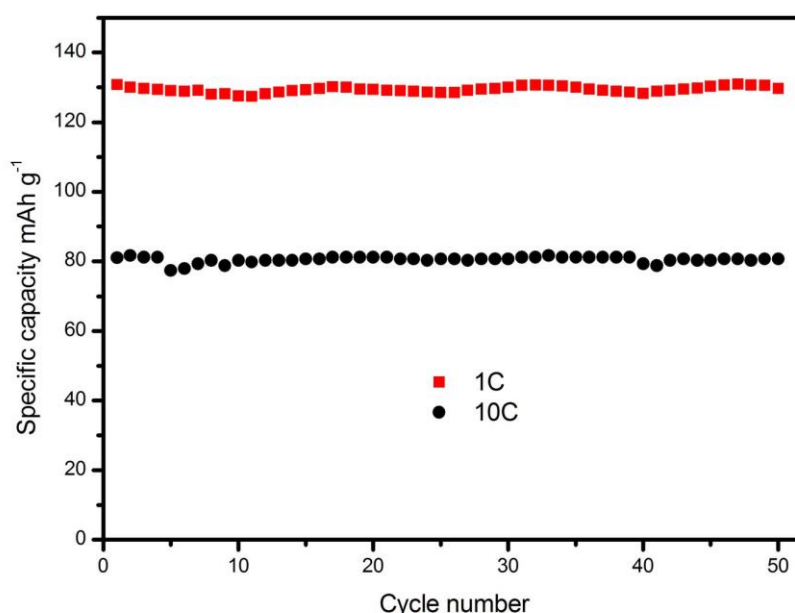

Figure 6. The cycling performances of 4wt% CNTs at 1C and 10C rates

The cycling performance of the LFP/CNTs (4wt%) sample at room temperature also interesting, as shown in Fig.6. It can be seen that the charge-discharge specific capacity has any remarkable reducing after 50 cycles at 1C and 10C rates. Apart from the confirmation of the superior performance, the plot provides evidence of the good cycling stability of this sample. During the process of lithium intercalation/deintercalation, a combination of polarizations, such as electrolyte polarization, electron-transfer resistance within the electrode, causes the overall cell-voltage [29]. Therefore, the reason may be caused by the particle size of LFP that shorten the path of the transport of lithium ion and reduce the polarization resistance from the process of electronic transfer [30–32].

4. CONCLUSION

LFP has been prepared by hydrothermal method with the assistance of EG and the LFP/CNTs composite is synthesized in the process of final heat treatment added different percentages of CNTs.

This study discuss that the different amount of CNTs impact on the electrochemical performance. The tests show that the LFP/CNTs (4wt%) has the highest discharge specific capacity, and the addition has no effect on the structure of pure LFP. The discharge capacity of LFP/CNTs (4wt%) is observed as 154.6mAh/g, which exhibit the highest initial discharge capacity, the capacity retention is 90.9%. The particle size of LFP, prepared by hydrothermal method with the assistance of EG, is short and the 3D network structure improve the conductivity performance of the battery.

References

1. W. Shang, L. Kong, X. Ji, *Solid State Sci*, 38 (2014) 79.
2. F. Yu, L. Zhang, L. Lai, M. Zhu, Y. Guo, L. Xia, P. Qi, G. Wang, B. Dai, *Electrochimica Acta*, 151 (2015) 240.
3. D. Rangappa, K. Sone, T. Kudo, I. Honma, *J. Power Sources,* 195 (2010) 6167.
4. A.K. Padhi, *J. Electrochem. Soc*, 144 (1997) 1188.
5. D.H. Nagaraju, M. Kuezma, G.S. Suresh, *J. Mater. Sci*, 50 (2015) 4244.
6. H. Gong, H. Xue, T. Wang, J. He, *J. Power Sources*, 318 (2016) 220.
7. H. Wu, Q. Liu, S. Guo, *Nano-Micro Lett*, 6 (2014) 316.
8. P.-L. Kuo, C.-H. Hsu, H.-T. Chiang, J.-M. Hsu, *J. Nanoparticle Res*,15 (2013) 1966.
9. V.H. Nguyen, H.-B. Gu, *J. Appl. Electrochem*, 44 (2014) 1153.
10. A. Andersson, *Solid State Ion,* 130 (2000) 41.
11. J. Chen, N. Zhao, G.-D. Li, F.-F. Guo, J. Zhao, Y. Zhao, T. Jia, F. Fu, J. Li, *Mater. Res. Bull*, 73 (2016) 192.
12. P. Swain, M. Viji, P.S.V. Mocherla, C. Sudakar, J. *Power Sources*, 293 (2015) 613.
13. Y. Li, D. Fu, X. Zhang, S. Qiu, C. Qin, *J. Mater. Sci. Mater. Electron*, 27 (2016) 4417.
14. C. Gong, Z. Xue, S. Wen, Y. Ye, X. Xie, *J. Power Sources*, 318 (2016) 93.
15. X. Lei, H. Zhang, Y. Chen, W. Wang, Y. Ye, C. Zheng, P. Deng, Z. Shi, *J. Alloys Compd*, 626 (2015) 280.
16. F.-Y. Su, C. You, Y.-B. He, W. Lv, W. Cui, F. Jin, B. Li, Q.-H. Yang, F. Kang, *J. Mater. Chem*, 20 (2010) 9644.
17. R. Muruganantham, M. Sivakumar, R. Subadevi, S. Ramaprabhu, N.-L. Wu, *Electron. Mater. Lett*, 11 (2015) 841.
18. B. Wang, A. Liu, W.A. Abdulla, D. Wang, X.S. Zhao, *Nanoscale*, 7 (2015) 8819.
19. D. Choi, D. Wang, V.V. Viswanathan, I.-T. Bae, W. Wang, Z. Nie, J.-G. Zhang, G.L. Graff, J. Liu, Z. Yang, T. Duong, *Electrochem. Commun*, 12 (2010) 378.
20. G. Wu, Y. Zhou, X. Gao, Z. Shao, *Solid State Sci*, 24 (2013) 15.
21. G. Wu, R. Ran, B. Zhao, Y. Sha, C. Su, Y. Zhou, Z. Shao, *J. Energy Chem*, 23 (2014) 363.
22. L. Tan, Q. Tang, X. Chen, A. Hu, W. Deng, Y. Yang, L. Xu, *Electrochimica Acta*, 137 (2014) 344.
23. G. Wang, Z. Ma, G. Shao, L. Kong, W. Gao, *J. Power Sources*, 291 (2015) 209.
24. N. Bai, K. Xiang, W. Zhou, H. Lu, X. Zhao, H. Chen, *Electrochimica Acta*, 191 (2016) 23.
25. P.-L. Kuo, C.-H. Hsu, H.-T. Chiang, J.-M. Hsu, *J. Nanoparticle Res*, 15 (2013).
26. J. Reed, G. Ceder, *Chem. Rev*. 104 (2004) 4513.
27. A. Gören, C.M. Costa, M.M. Silva, S. Lanceros-Méndez, *Compos. Part B Eng*, 83 (2015) 333.

28. H. Göktepe, H. Şahan, Ş. Patat, *Int. J. Hydrog. Energy*, 41 (2016) 9774.
29. S.W. Oh, H.J. Bang, S.-T. Myung, Y.C. Bae, S.-M. Lee, Y.-K. Sun, *J. Electrochem. Soc*, 155 (2008) 414.
30. W. Yang, J. Liu, X. Zhang, L. Chen, Y. Zhou, Z. Zou, *Appl. Energy*, (2016).
31. H. Liao, H. Zhang, H. Hong, Z. Li, G. Qin, H. Zhu, Y. Lin, *J. Membr. Sci*, 514 (2016) 332.
32. W.C. Chueh, F. El Gabaly, J.D. Sugar, N.C. Bartelt, A.H. McDaniel, K.R. Fenton, K.R. Zavadil, T. Tyliszczak, W. Lai, K.F. McCarty, *Nano Lett*, 13 (2013) 866.